Annals of Nuclear Medicine Vol. 18, No. 4, 315–322, 2004

Attenuation correction using asymmetric fanbeam transmission CT on two-head SPECT system

Akihiro KOJIMA,* Seiji TOMIGUCHI,** Koichi KAWANAKA,** Daisuke UTSUNOMIYA,** Shinya SHIRAISHI,** Takeshi NAKAURA,** Noboru KATSUDA,** Masanori MATSUMOTO,*** Yasuyuki YAMASHITA,** Nobutoku MOTOMURA**** and Takashi ICHIHARA****

*Institute of Resource Development and Analysis, Kumamoto University
**Department of Radiology, Kumamoto University School of Medicine
***Course of Radiological Sciences, Kumamoto University School of Health Sciences
****Toshiba Medical Systems Corporation

For transmission computed tomography (TCT) systems using a centered transmission source with a fan-beam collimator, the transmission projection data are truncated. To achieve sufficiently large imaging field of view (FOV), we have designed the combination of an asymmetric fan-beam (AsF) collimator and a small uncollimated sheet-source for TCT, and implemented AsF sampling on a two-head SPECT system. The purpose of this study is to evaluate the feasibility of our TCT method for quantitative emission computed tomography (ECT) in clinical application. Sequential Tc-99m transmission and Tl-201 emission data acquisition were performed in a cardiac phantom (30 cm in width) with a myocardial chamber and a patient study. Tc-99m of 185 MBq was used as the transmission source. Both the ECT and TCT images were reconstructed with the filtered back-projection method after scatter correction with the triple energy window (TEW) method. The attenuation corrected transaxial images were iteratively reconstructed with the Chang algorithm utilizing the attenuation coefficient map computed from the TCT data. In this AsF sampling geometry, an imaging FOV of 50 cm was yielded. The attenuated regions appeared normal on the scatter and attenuation corrected (SAC) images in the phantom and patient study. The good quantitative accuracy on the SAC images was also confirmed by the measurement of the Tl-201 radioactivity in the myocardial chamber in the phantom study. The AsF collimation geometry that we have proposed in this study makes it easy to realize TCT data acquisition on the two-head SPECT system and to perform quantification on Tl-201 myocardial SPECT.

Key words: asymmetric fan-beam collimator, attenuation correction, transmission computed tomography, two-head SPECT system, Tl-201 myocardial SPECT

INTRODUCTION

Thallium-201 (Tl-201) single-photon emission computed tomography (SPECT) is a well established imaging modality for evaluation of the presence and extent of coronary artery disease. However, photon attenuation by breast, diaphragm and right ventricle degrades the quantitative accuracy of Tl-201 SPECT images.[1–3] It also results in a degradation of image quality due to image artifacts and distortions.[3] To address these problems, proper attenuation correction for Tl-201 SPECT images is needed.[3]

Measurement of attenuation distribution using transmission computed tomography (TCT) scan is the most promising method for attenuation correction.[3–13] The desirable way is to apply the TCT to the SPECT system that also acquires the emission computed tomography (ECT) data, either simultaneously or sequentially, to assure registration of these two sets of images.

Among many TCT approaches, from parallel-beam to

Received December 8, 2003, revision accepted March 8, 2004.

For reprint contact: Akihiro Kojima, Ph.D., Institute of Resource, Development and Analysis, Kumamoto University, 2–2–1 Honjo, Kumamoto 860–0811, JAPAN.

E-mail: akojima@kaiju.medic.kumamoto-u.ac.jp

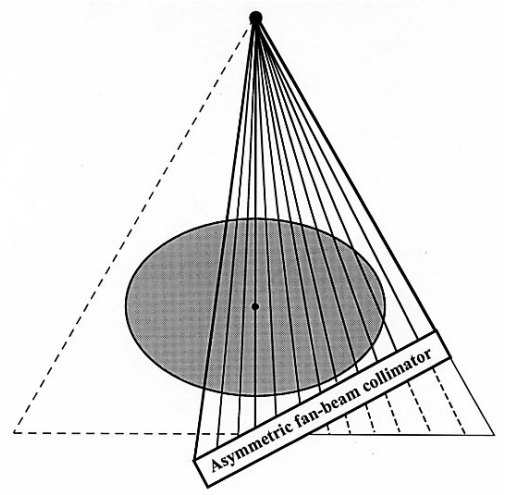

Fig. 1 The AsF geometry and the half FOV of the SF geometry. A triangle with slanted lines indicates the AsF geometry, while a broken line triangle on the left divided by the line from the focus to the COR indicates the half FOV of the SF geometry. The AsF transmission projection data are transferred to the half FOV of the SF transmission data by extending the acquired projection rays.

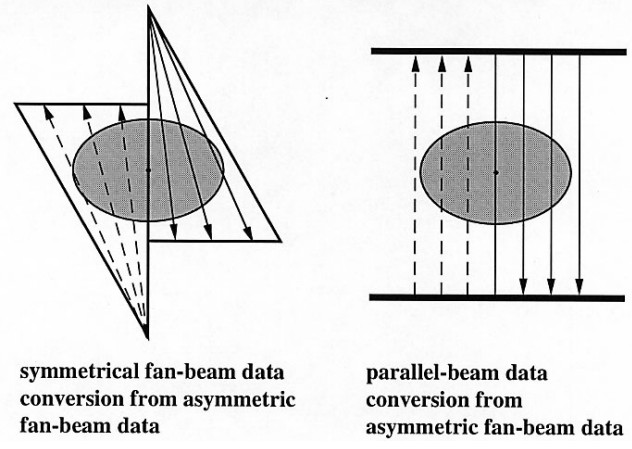

Fig. 2 Schematic display of the AsF transmission geometry. The right and left triangles indicate the half SF projections acquired when the whole system is rotated to the opposite view. The arrows represent the direction of the transmission rays. Each truncated projection of the AsF is implemented by a corresponding opposing projection to complete the sampling coverage of the FOV.

cone-beam geometries, a fan-beam TCT technique has many promising features for clinical applications.[8–12] The advantages are the technical simplicity of its implementation, the high count-rate level without loss of spatial resolution and the reduction in scatter photon. However, the imaging field of view (FOV) realized with fan-beam TCT on SPECT systems is not large enough to encompass the thorax for most patients. For the conventional symmetric fan-beam geometries, with a focal distance between 60 and 100 cm, the corresponding imaging FOV formed is between 25 and 31 cm on a typical Anger camera of 40 cm useful FOV.[13] Small imaging FOV results in truncation in many projections. Using these truncated projection data for reconstruction with the conventional convolution backprojection algorithm, high intensity edge artifacts would show up in the peripheral FOV and quantitative inaccuracy would be generated.[3,9] To solve this problem, iterative reconstruction techniques such as maximum-likelihood algorithms are necessary.[8] To utilize commonly existing hardware and software, the proper way to compensate for the effect of attenuation is to fully define the attenuation map in the entire imaging volume. Chang et al.[13] reported that the 37 cm imaging FOV was yielded using an asymmetric fan-beam (AsF) collimator on a three-head SPECT system. This sampling technique effectively extended the imaging FOV to practical clinical sizes for TCT, but much larger imaging FOV was necessary to image nearly all patients.

To achieve sufficiently large imaging FOV, we have designed AsF collimators, used in combination with a small uncollimated sheet transmission source for TCT, and implemented AsF sampling on a two-head SPECT system. The purpose of this study is to evaluate the feasibility of our methods for clinical application.

MATERIALS AND METHODS

Theory

To provide sampling coverage for the region missed by a symmetric fan-beam (SF) collimator, one can use an AsF collimator to trade peripheral coverage on one side for the other side. In AsF sampling, the size of realizable FOV is defined by the outside edge of the asymmetric fan, provided the central region is also properly sampled. The inside edge of the asymmetric fan should extend beyond the center of rotation (COR) so that there is some overlap between the two opposing sampling asymmetric fan-beams in the central region. This sampling scheme focuses on only half of the intended FOV in each projection. As shown in Figure 1, AsF data are transferred to a half of SF data which corresponds to the right part of SF data divided by a line drawn from the focus of AsF to the surface of the AsF collimator through the COR. The right half of FOV can be sampled from this projection. The remaining half of the FOV will be sampled from an opposing projection after 180° detector rotation (Fig. 2). This scheme thus requires a full 360° rotation to meet the minimum sampling requirement. This AsF scheme can be used since transmission projections acquired from opposite directions are identical. This AsF geometry yields an imaging FOV of 50 cm on a 55 cm useful FOV of the two-head SPECT system.

System overview

To examine the feasibility of AsF sampling, we have

designed an AsF lead collimator and a small uncollimated sheet-source assembly. In the two-head SPECT system used in this study, the maximum radius of rotation (ROR) was 31 cm. To realize the 50 cm imaging FOV for the TCT with 5 cm sheet source in width, we made the 68.8 cm focal length of the AsF collimator. The AsF collimator consisted of progressively slanted hexagonal holes, which were focused on a line located 68.8 cm from the surface of the top of collimator. The maximum diameter of the hexagonal holes was 1.8 mm and collimator thickness was 4.0 cm. Volume sensitivity of this collimator for a Tl-201 emission source was 90 kcps/(kBq/m*l*)/cm, and tomographic spatial resolution was 20 mm FWHM at the COR. We made a small sheet source assembly consisting of an uncollimated plate source (5 × 20 cm in size) and its holder. The purpose of the sheet source holder was not only to hold the sheet source but also to provide a shielded enclosure for the sheet source except in the direction of the object being scanned.

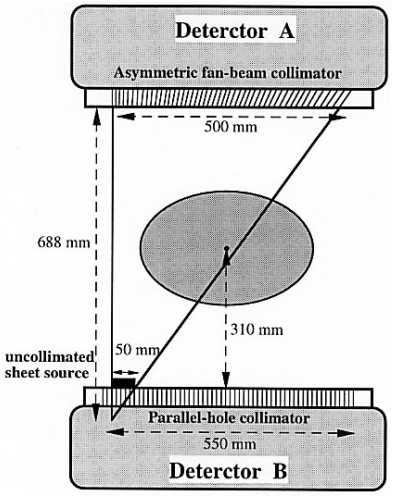

Fig. 3 A schematic display of the two-head SPECT system. A small uncollimated sheet source and a source holder are mounted on the edge of the Detector B. The imaging FOV of 50 cm is realized on this system.

The main components were mounted on a two-head SPECT system (GCA 7200A, Toshiba, Japan). For TCT and ECT data acquisitions, the AsF collimator was mounted on the Detector A as shown in Figure 3. A transmission source holder including a small uncollimated sheet source was mounted at the edge of the opposite Detector B at a fixed circular orbit of 31 cm ROR. The volume FOV for TCT imaging is a cylinder with diameter 50 cm and axial length 20 cm.

Phantom study

A cardiac phantom (long axis 30 cm, short axis 20 cm, height 21 cm) (Kyoto Kagaku Corporation, Kyoto, Japan) used in this study consisted of mediastinum, lung part, spinal part, and a heart that could be placed in the mediastinum (Fig. 4A). A lung part was filled with Styrofoam to simulate the photon attenuation properties of the lung tissue and spinal part consisted of the Teflon spine to simulate those of the bone tissue. The heart was placed inside the mediastinum. This heart consisted of left and

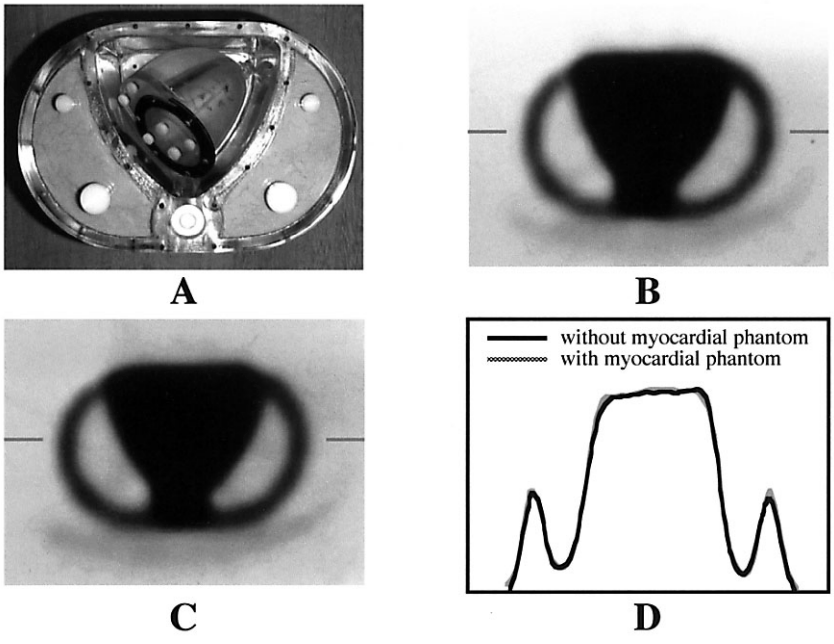

Fig. 4 The cardiac phantom with the heart part (A). The TCT images of the cardiac phantom without (B) and with (C) the heart part filled with Tl-201 in its myocardial chamber and the profile curves corresponding to each image (D). Both images and profile curves are similar in appearance.

right ventricles. Left ventricle was composed of two concentric chambers separated by 1.0 cm. The space between the concentric chambers simulated the myocardial chamber and could be filled with radioactive solution. A defect of 2 cm in diameter was inserted in the anterolateral portion of this chamber. In this study, this space was filled with 38.2 MBq of Tl-201 solution. The right ventricle was made of a single chamber to simulate the right ventricle and could be attached to the left ventricle. The mediastinum of the cardiac phantom except for the heart, the inner concentric chamber of the left ventricle and right ventricle of the heart were filled with non-radioactive water. In the phantom study, three water bags (750 m*l*, 300 m*l* and 75 m*l*) to simulate the breast were placed in front of the cardiac phantom to enhance non-uniformity of attenuation.

For the cardiac phantom with or without the heart containing Tl-201, transmission projection data were collected in 128 × 128 matrices using the AsF collimator and the small uncollimated sheet-source with 185 MBq of Tc-99m. A total of 60 views over 360° were acquired. The acquisition time for each view was 15 sec. The incident flux data were measured by collecting a static image of the sheet source without phantom. A count-rate 50 kcps was obtained. Emission projection data were collected following the TCT imaging in 128 × 128 matrices using two general-purpose parallel hole (GP) collimators. A total of 60 views over 360° (30 views over 180° for each detector) were acquired. Each view was acquired for 30 sec in a body contouring acquisition.

One set of three energy windows was placed over the photopeak of Tl-201 or Tc-99m. The main window for Tl-201 was set at the center of 73 keV with the 47% energy window. Two sub-windows of 7% were set at both sides of the main window for Tl-201. The main window for Tc-99m was set at the center of 140 keV with the 20% energy window. Two sub-windows of 7% were set at both sides of the main window for Tc-99m.

The steps in reconstructing the TCT image were as follows:

1. The scatter component for Tc-99m in TCT data (AsF data) was removed pixel by pixel using the modified triple energy window (TEW) method.[17]
2. Attenuation coefficient projection (ACP) images for AsF data were formed by taking the natural logarithm of the incident flux-to-transmission scan ratio at each angle.
3. ACP images were changed in those for a half of a symmetric fan-beam (half SF) data using the method described in the theory.
4. This half SF data were then transformed to the parallel beam (PB) transmission data.
5. These PB data were subjected to 2D Butterworth filter processing before reconstruction (cutoff frequency of 0.14 cycle/cm and order of 8).
6. These TCT images were reconstructed using a filtered backprojection with a Ramp filter, and the slice thickness was 4.3 mm.
7. Since the transmission data were acquired with 140 keV photons and emission data with 71 keV photons, the measured attenuation coefficient map was scaled by the ratio of attenuation coefficient of water at 71 keV divided by that at 140 keV.

The steps in reconstructing the ECT image were as follows:

1. The scatter component of Tl-201 was removed pixel by pixel using the TEW method.
2. The emission projection data were subjected to 2D Butterworth filter processing before reconstruction (cut-off frequency of 0.28 cycle/cm and order of 8).
3. The ECT images were reconstructed using a filtered backprojection with a Ramp filter, and the slice thickness was 4.3 mm.

In ECT data acquisition, four images, such as those without scatter and attenuation correction, with only scatter correction, with only attenuation correction and with scatter and attenuation corrections, were reconstructed. The attenuation correction was performed with a single iteration Chang algorithm using the attenuation map.

To evaluate the accuracy for the quantification of radioactivity of Tl-201 in the myocardial phantom, the measured radioactivity in the myocardial phantom was obtained using the cross-calibration factor in the phantom study with water bags that simulated the breast.

Cross-calibration factor (kBq · sec/ count) was calculated using the total counts of the SPECT image including the whole range of a fine cylinder (5 mm in diameter, 50 mm long) filled with Tl-201 in air, the known radioactivity, and the acquisition time: cross calibration factor (kBq · sec/ count) = radioactivity (kBq) × acquisition time (sec)/ counts.

Patient study

Informed consent was obtained prior to the study. In a Tl-201 stress study, a 66-year-old female with ischemia in the septal wall of the left ventricle was subjected to cycling exercise. At the peak exercise, a 111 MBq of Tl-201 chloride was injected intravenously and exercise continued at the same level for 60 sec. Following this exercise, the patient was transferred to the two-head SPECT system for the emission data acquisition. The time interval between the injection and the onset of the ECT was less than 10 min. The emission projection data were acquired by the same technique used in the phantom study with the two GP collimators.

After collection of the emission data, one GP collimator on Detector A was changed to the AsF collimator and the small uncollimated sheet-source with 185 MBq of Tc-99m was installed. Without moving the patient, the transmission data were acquired in 128 × 128 matrices and in 60 views over 360° rotation. At 5 sec/view, the total transmission scan time was 6 min.

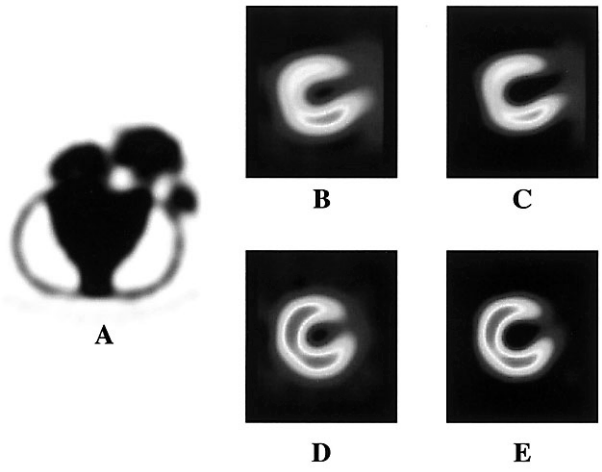

Fig. 5 The TCT image of the cardiac phantom with three water bags (A) and the short axial images of the myocardial chamber (B, C, D, and E). The shape of the myocardial chamber is distorted and the attenuated radioactivity distribution is observed in the anterior and inferior wall on the images without the attenuation correction: without (B) and with (C) the scatter correction. The image distortion in shape is restored and the attenuation is compensated with the attenuation correction: without (D) and with (E) the scatter correction. A defect in the anterolateral wall is more clearly visualized on scatter corrected images (C and E).

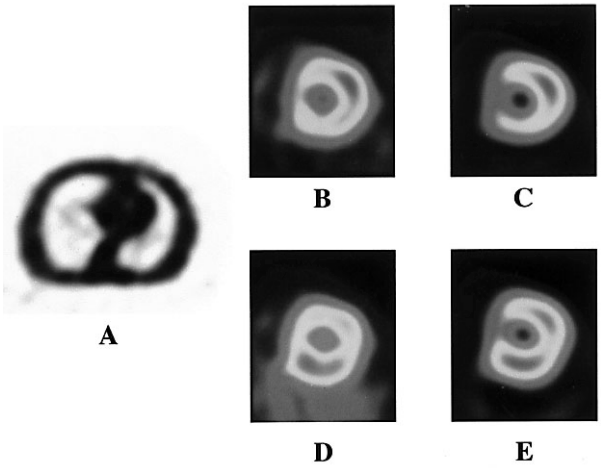

Fig. 6 The TCT image of a female patient with effort angina pectoris (A) and the short axial images (B–E) of the stress Tl-201 SPECT for the same patient are shown. Mild decrease in Tl-201 radioactivity was observed in the septal wall and inferior wall on the image without either the scatter or attenuation corrections (B). Scatter correction alone enhanced reduced radioactivity in these regions (C). Overcorrection was observed in the inferior wall with the attenuation correction alone (D). Uniform distribution in Tl-201 radioactivity except for the septal wall was obtained with both the scatter and attenuation corrections (E).

Table 1 Comparison between the estimated Tl-201 radioactivity and the true Tl-201 radioactivity in the myocardial chamber of the cardiac phantom

Estimated radioactivity (MBq)				True radioactivity (MBq)
NC	SC	AC	SAC	
9.07	5.59	59.87	36.63	38.18

NC: without scatter and attenuation corrections, SC: with scatter correction alone
AC: with attenuation correction alone, SAC: with scatter and attenuation corrections

Table 2 Comparison of the myocardial SPECT values of the patient in the Tl-201 clinical study

Myocardial SPECT value ratio*			
NC	SC	AC	SAC
0.329	0.235	1.504	1

NC: without scatter and attenuation corrections, SC: with scatter correction alone
AC: with attenuation correction alone, SAC: with scatter and attenuation corrections
* Each ratio is normalized with the SPECT value by SAC.

After the transmission scan, the incident flux image was obtained for 5 min. The same reconstruction and processing techniques used in the phantom study were applied to the patient data.

RESULTS

Phantom study

Two different TCT reconstructed images of the cardiac phantom were presented in Figures 4B and 4C. The heart, where the myocardial chamber was filled with Tl-201 water solution, was not visualized in the TCT reconstructed cardiac phantom images. The TCT reconstructed cardiac phantom images without the heart were similar in appearance to those with the heart. The attenuation coefficient of water for Tc-99m in the mediastinal part was 0.151/cm on the TCT reconstructed image without the heart and 0.148/cm on that with the heart, respectively. Horizontal profiles drawn through the mediastinal part of the TCT images without and with the heart were also shown in Figure 4D. Both profiles were also similar in shape.

ECT reconstructed images of the cardiac phantom with the water bags to simulate the breasts were demonstrated in Figure 5. Decrease in radioactivity distribution was observed in the anterior and inferior wall of the myocardial chamber on the short axial images without attenuation correction (Figs. 5B and 5C). Decrease in radioactivity in the anterior wall and distortion in circular shape were caused by the water bags. The defect in the anterolateral wall was more clearly visualized on the short axial image with scatter correction than on that without scatter correction. Attenuated radioactivity distribution and the

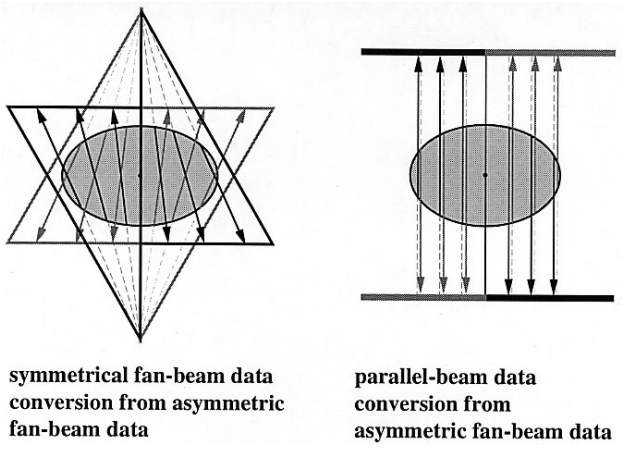

Fig. 7 Schematic display of the AsF emission geometry using one AsF collimator. When a full 360° rotation is performed on this system, the emission data of the half of the object (*black lines*) can be collected. To complete the sampling coverage of the object, another different-angle AsF collimation (*gray lines*) is necessary. The arrows show the direction of the emission rays.

distortion in shape observed on the short axial images without attenuation correction were restored on those with attenuation correction (Figs. 5D and 5E).

Estimated radioactivities of Tl-201 in the myocardial chamber calculated using the cross-calibration factor are indicated in Table 1. Total radioactivity in the myocardial chamber was measured by sum of the radioactivity in the region of interest placed on all short axial images. The total radioactivity was overestimated for the short axial images with only attenuation correction, and in contrast underestimated with only scatter correction. Accurate quantification for the radioactivity was made with both scatter and attenuation corrections.

Patient study

A TCT reconstructed image of a patient through the heart was demonstrated in Figure 6A. There was no truncation artifact seen on this image. The short axial images of the left ventricle of this patient were also shown in Figure 6. The regions with the mildly decreased counts were observed in the septal and inferior wall when no attenuation or scatter corrections were employed (Fig. 6B). The scatter correction alone enhanced the degree of the count-reduction in these walls (Fig. 6C). Without the scatter correction, overcorrection in the inferior wall resulted from the attenuation correction (Fig. 6D). However, relatively uniform count-distribution in the myocardial regions was obtained with both the scatter and the attenuation corrections except for the ischemic lesion of the septal wall (Fig. 6E). The SPECT values, calculated from all short axial images of the patient's myocardium, are listed in Table 2. The same effect of the corrections as the result of the phantom is seen.

DISCUSSION

For transmission computed tomography (TCT) systems using a centered transmission source with a fan-beam collimator, the transmission projection data may be truncated, and iterative reconstruction methods may be required to fill in the truncated information. To address this problem, we have designed an asymmetric fan-beam (AsF) sampling scheme to extend the FOV for clinical TCT imaging with a wide range of patient bodies on a two-head SPECT system. Two-head gamma cameras are more widely and more commonly used for SPECT than three-head ones. Our TCT imaging technique requires only a specially designed AsF collimator and a narrow uncollimated sheet source with a small amount of radioactivity.

To make an accurate map of the distribution of attenuation coefficient in the thorax, the scatter photons from the transmission source itself and cross-contaminated photons from the emission source must be eliminated from the transmission projection data. In this study, Tc-99m was utilized as the transmission source and Tl-201 as the emission source. The TEW scatter compensation method is a well established one for the scatter correction of Tc-99m.[14–16] This method was used for the correction of scatter photon and cross-contamination from Tl-201 in the Tc-99m energy window.[17] Co-workers in this study[17] indicated that the TEW method was effective for the elimination of scatter of Tl-201 and the crosstalk from the Tc-99m transmission source in the Tl-201 emission projection data. In our phantom study, the TCT reconstructed images of the cardiac phantom including the Tl-201 emission source in the mediastinal part were similar to those without Tl-201 emission source. Although the amount of cross-contamination of the Tl-201 in the Tc-99m energy window may be small enough to be ignored, this method is practically useful for the cross-contamination correction. This means that accurate attenuation maps can be obtained for even the patients having Tl-201.

Collimation on the transmission source provides substantial reduction in dose to the patient and substantial scatter reduction in TCT data acquisition.[13] We did not use the collimated transmission source. However, in our patient study, the small uncollimated sheet-source filled with 185 MBq of Tc-99m was employed as a transmission source and the total TCT data acquisition time was 6 min. The amount of Tc-99m radioactivity is small and the scan time is very short, as compared with the TCT imaging using an uncollimated Tc-99m flood source of 925 MBq and scan time of 20 min, which causes the patient's exposure dose of 0.06 mSv.[18] So the patient's exposure dose by our TCT data acquisition seems to be at an acceptable level for clinical use.

The AsF collimator on the detector provides substantial scatter reduction in TCT data acquisition. In addition, for removing the scatter photon in the TCT projection data,

the TEW method was applied. In the phantom study, a good quantitative result in measurement of the Tl-201 radioactivity in the myocardial chamber was obtained when performing the attenuation correction following the scatter correction with the TEW method. Therefore, our TCT procedure with AsF collimator is considered to be suitable for clinical use.

The AsF collimator is capable of not only collecting TCT data but also acquiring ECT data like symmetric fan-beam collimators. As shown in Figure 2, for an AsF collimator only half of a full ECT data can be also sampled with a full 360° detector rotation. The remaining ECT data must be obtained using a reverse-angle AsF collimator (Fig. 7). Therefore, both left-angle and right-angle AsF collimators are necessary for the complete sampling of the 360° ECT data acquisition together.

The simultaneous transmission and emission data acquisition is an efficient clinical study. The simultaneous TCT and ECT operation using the AsF collimator for TCT scan was not the optimal arrangement on a three-head SPECT system.[13] This was because AsF sampling on a three-head SPECT system required the detector with the AsF collimator and the side detector behind the source holder to be pulled outward to the specified distance, and because the line source assembly blocked a portion of the side detector. For the simultaneous TCT and ECT data acquisition using the AsF collimator on the two-head SPECT system, the combination of either left- or right-angle AsF and one parallel-hole collimators, and the combination of one left-angle and one right-angle AsF collimators are available (Fig. 7). In case of using a parallel-hole collimator for the ECT data acquisition, it is preferable that the ROR of the parallel-hole collimator be shorter for the quality of ECT image. Therefore, to maintain the full FOV of the AsF collimator for TCT scan, a wider sheet source assembly (~11 cm) is inevitably required not to block off the emission ray. In the circumstances, a line array source that consists of a finer tube on a thinner board may be available.[19] Then, the cross-contamination from photons for TCT to the energy window for ECT must be removed successfully. For use of two different-angle AsF collimators as shown in Figure 7, TCT data can be acquired with one of two AsF collimators and ECT data collected by both collimators with the maximum ROR (each 31 cm), simultaneously. However, we think that there are some problems in this method. One problem is a lower sensitivity of the AsF collimator because of a limited FOV as compared with the parallel-hole collimator. In our results, the sensitivity of the AsF collimator was 90 kcps/(kBq/m*l*)/cm for a Tl-201 line source, while the GP parallel-hole collimator's sensitivity was 200 kcps/(kBq/m*l*)/cm. Furthermore, the periphery of the useful FOV of the detector tends to be non-uniform as compared with the center of the useful FOV. This non-uniformity in the peripheral FOV may result in the degradation of the emission reconstructed images because the central object such as the heart is projected to the peripheral FOV in the AsF sampling geometry.

So, we have the alternative of the sequential or simultaneous TCT and ECT data acquisitions in respect of the practical use of the AsF collimators proposed here. At the moment, our thinking is as follows: There are several advantages in such a sequential method used in this study over the simultaneous method. First, the emission scan can be performed with optimal sensitivity and resolution because all detectors are brought in close to the object. Second, the problematic crosstalk between the emission and transmission photons can be effectively handled. Third, the transmission data acquisition can be completed in a short time without changing the patient position. Then the patient exposure from the transmission source is less than that from using the simultaneous technique. Finally, the total acquisition time using the sequential method is 30 min, which is nearly the same as when the simultaneous method is applied.

In conclusion, the TCT imaging using the AsF collimator on the two-head SPECT system used in this study can provide accurate quantification of the Tl-201 radioactivity distribution in the thorax and is feasible for clinical use.

REFERENCES

1. Eisner RL, Tamas MJ, Clononger K, Shonkoff D, Oates JA, Gober AM, et al. Normal SPECT Thallium-201 bull's-eye display: gender differences. *J Nucl Med* 1988; 29: 1901–1909.
2. Manglos SH, Thomas FD, Gagne GM, Hellwig BJ. Phantom study of breast tissue attenuation in myocardial imaging. *J Nucl Med* 1993; 34: 992–996.
3. King MA, Tsui BMW, Pan TS. Attenuation compensation for cardiac single-photon emission computed tomographic imaging: Part 1. Impact of attenuation and methods of estimating attenuation maps. *J Nucl Cardiol* 1995; 2: 513–524.
4. Greer KL, Harris CC, Jaszczak RJ, Coleman RE, Hedlund LW, Floyd CE, et al. Transmission computed tomography data acquisition with a SPECT system. *J Nucl Med Tech* 1987; 15: 53–56.
5. Bailey DL, Hutton BF, Walker PJ. Improved SPECT using simultaneous emission and transmission tomography. *J Nucl Med* 1987; 28: 844–851.
6. Tsui BMW, Gullberg GT, Edgerton ER, Ballard JG, Perry JR, McCartney WH, et al. Correction of nonuniform attenuation in cardiac SPECT imaging. *J Nucl Med* 1989; 30: 497–507.
7. Frey EC, Tsui BMW, Perry JR. Simultaneous acquisition of emission and transmission data for improved Thallium-201 cardiac SPECT imaging using a Technetium-99m transmission source. *J Nucl Med* 1992; 33: 2238–2245.
8. Tung CH, Gullberg GT, Zeng GL Christian PE, Datz FL, Morgan HT. Non-uniform attenuation correction using simultaneous transmission and emission converging tomography. *IEEE Trans Nucl Sci* 1992; 39: 1134–1143.
9. Jaszczak RJ, Gilland DR, Hanson MW, Jang S, Greer KL, Coleman RE. Fast transmission CT for determining attenu-

ation maps using a collimated line source, rotatable air-copper-lead attenuators and fan-beam collimation. *J Nucl Med* 1993; 34: 1577–1586.
10. Ficaro EP, Fessler JA, Rogers WL, Schwaiger M. Comparison of Americium-241 and Technetium-99m as transmission sources for Thallium-201 SPECT imaging of the heart. *J Nucl Med* 1994; 35: 652–663.
11. Ficaro EP, Fessler JA, Ackermann RJ, Rogers WL, Corbett JR, Schwaiger M. Simultaneous transmission-emission Thallium-201 cardiac SPECT: Effect of attenuation correction on myocardial tracer distribution. *J Nucl Med* 1995; 36: 921–931.
12. Gullberg GT, Zeng GL, Datz FL, Christian PE, Tang CH, Morgan HT. Review of convergent beam tomography in single photon emission computed tomography. *Phys Med Biol* 1992; 37: 507–534.
13. Chang W, Loncaric S, Huang G, Sanpitak P. Asymmetric fan transmission CT on SPECT systems. *Phys Med Biol* 1995; 40: 913–928.
14. Ogawa K, Harata Y, Ichihara T, Kubo A, Hashimoto S. A practical method for position-dependent Compton scatter correction in SPECT. *IEEE Trans Med Imag* 1991; 10: 408–412.
15. Ichihara T, Ogawa K, Motomura N, Kubo A, Hashimoto S. Compton-scatter compensation using the triple energy window method for single and dual isotope SPECT. *J Nucl Med* 1993; 34: 2216–2221.
16. Ogawa K, Ichihara T, Kubo A. Accurate scatter correction in single photon emission CT. *Ann Nucl Med* 1994; 6: 145–150.
17. Ichihara T, Motomura N, Ogawa K, Hasegawa H, Hashimoto J, Kubo A. Evaluation of SPECT quantification of simultaneous emission and transmission imaging of the brain using a multidetector SPECT system with the TEW scatter compensation method and fan-beam collimation. *Eur J Nucl Med* 1996; 23: 1292–1299.
18. Ichihara T, Maeda H, Yamakado K, Motomura N, Matsumura K, Takeda K, et al. Quantitative analysis of scatter- and attenuation-compensated dynamic single-photon emission tomography for functional hepatic imaging with a receptor-binding radiopharmaceutical. *Eur J Nucl Med* 1997; 24: 59–67.
19. Kojima A, Matsumoto M, Tomiguchi S, Katsuda N, Yamashita Y, Motomura N. Accurate scatter correction for transmission computed tomography using an uncollimated line array source. *Ann Nucl Med* 2004; 18: 45–50.